

# A generalised microbial cell model for methane biosignature predictions

Arwen. E. Nicholson<sup>1\*</sup>, Nathan J. Mayne<sup>1</sup>

<sup>1</sup>*Department of Physics and Astronomy, University of Exeter*

Accepted XXX. Received YYY; in original form ZZZ

## ABSTRACT

The majority of potentially habitable planets detected to date are likely quite different to Earth, for example, being larger in radius and mass, differing rotation rates and with host star spectra unlike the Sun. Therefore the first alien life detected will potentially be living in conditions not found on our planet. This necessitates a generalised approach to modelling biology that can be applied to numerous planetary scenarios, built on fundamental knowledge of life on Earth, but not limited by it. Here, we explore a generalised model of a microbial cell, whose metabolic rate is governed by thermodynamics and substrate diffusion across its cell wall. We model a single-species biosphere consisting of methane producing microbes and determine how changing the cell size, cell death rate and biomass synthesis cost influence the biosignature on the planet - in this case methane. We discuss approaches to predicting upper estimates for the biosignature gas abundance and the applicability of the model to other metabolisms. This tool adds to the body of work attempting to grapple with the complexity of potential alien biospheres.

**Key words:** planets and satellites: atmospheres – planets and satellites: detection – astrobiology

## 1 INTRODUCTION

Numerous potentially habitable planets have been identified from observational data (Hill et al. 2023), however constraining the surface conditions of these exoplanets, let alone whether they host life, is enormously challenging (Montet et al. 2015; Foreman-Mackey et al. 2015; Cloutier et al. 2019; Tsiaras et al. 2019; Madhusudhan et al. 2020; Wogan et al. 2024; Shorttle et al. 2024). Developing our abiotic models of planetary atmospheres is of course crucial for understanding the observed data from any exoplanet. However life has the potential to strongly influence the atmosphere of its planet, for example acting to ‘erase’ certain abiotic features by transforming abiotically produced gases via their metabolisms (Lovlock 1965; Lovelock & Margulis 1974). Therefore, models including biology are key when considering potentially inhabited planets, not only for the identification of biosignatures, but also for understanding the wider planetary context of any observational data (Catling et al. 2018; Meadows et al. 2018; Krissansen-Totton et al. 2022; Arthur et al. 2025).

Given the range of planets discovered, it is likely that many potentially habitable planets experience very different surface conditions to those of Earth. For example, the most abundant planets in our galaxy have no solar-system analogue; these super-Earth and sub-Neptune planets have sizes and masses between those of their namesake solar system planets (Zhu et al. 2018; Livingston et al. 2026). A proposed subset of these planets are Hycean planets, which are characterised by global oceans and rich  $H_2$  atmospheres, and are thought to be potentially habitable (Madhusudhan et al. 2021, 2023a). Hycean planets would be significantly easier to observe than rocky Earth-like planets due to their extended atmosphere and so are of great interest for potential biosignature observations. Observational limitations also

mean that the smaller rocky planets that have been detected to date generally have orbits that are close in to host stars that are significantly smaller and cooler than the Sun (Sterzik et al. 2012; Fujii et al. 2018; Quanz et al. 2022; Snellen et al. 2021). Therefore, most potentially habitable exoplanets detected to date likely experience very different surface conditions than those on Earth due to factors such as the size and mass of the exoplanet, the orbital radius, and the stellar class of the host star. In our search for life in the galaxy, we are therefore likely searching for alien life that lives in a very different environment to any Earth-based life. This necessitates determining generalised properties of life that we can reasonably expect to find in alien biospheres. Towards this aim we propose a generalised biological model of methane producing microbes that can be used within a wide diversity of planetary contexts to understand a potential methane biosignature. The abiotic part of the model in this work is based on conditions found on early-Earth in a simplified manner. This part of the model acts as a testing-ground for our biological experiments so as to determine the qualitative impact on the planetary environment by changing various microbe parameters. To form predictions for a particular exoplanet a specific set up for the exoplanet in question, taking into account many factors such as planet size, mass, host star etc would be required as these can all impact how a biologically produced gas might accumulate in the planet’s atmosphere (Segura et al. 2005; Kiang et al. 2018).

In models of pre-Cambrian Earth it is standard to model microbial life by fixing the growth yield ratio of a metabolism (the energy required to build biomass) and the concentration down to which life can draw oceanic nutrients. These parameters, and a chosen burial rate, i.e. the biomass buried on the ocean floor and not recycled by heterotrophic life, determine the accumulation of by-products in the environment (Kharecha et al. 2005; Bruggeman & Bolding 2014). We build on this understanding to build a generalised cell model that

\* E-mail: arwen.e.nicholson@gmail.com

can be used in different planetary contexts to inform biosignature prediction models.

In this work, we consider properties of Earth-based life that we assume to be universal across the galaxy. We restrict this work to considering microbial chemosynthetic life and aim to expand this approach in later work to consider photosynthetic microbial and plant life. We assume that alien-life would utilise chemical potential gradients in their environment and obtain energy following the Gibbs free energy equation. We also assume that uptake of nutrients to an alien cell will be limited by diffusion uptake in some way. We consider free-living microbes, within an ocean, that obtain nutrients via diffusion across their cell membranes. While many lifeforms on Earth can move to seek out food they are still restricted by diffusion across cell membranes for their critical life processes e.g. uptake of  $CO_2$  through plant leaves or  $O_2$  diffusion across lung membranes in many animals. The ability to evolve and adapt is also typically included in definitions of life (Vitas & Dobovišek 2019) and therefore we assume competition for resources will occur within any alien biospheres.

To develop our model of a generalised cell model for a methane producing chemosynthetic microbial biosphere we use a quasi-realistic representation of the early-Earth. Forming biosignature predictions requires both plausible biological models and detailed models of the planetary environment. The same microbial life would result in different biosignatures under different planetary contexts. Here our focus is on the biological side of this puzzle and so as our planetary model is roughly based on early-Earth, the model as a whole cannot be used as-is for forming biosignature predictions. Any biosignature predictions for a potentially habitable planet will require bespoke modelling of the planetary environment. Numerous planetary parameters play a role in influencing the model behaviour, including the planet’s mass and atmospheric pressure. The depth, coverage and dynamics of the planet’s ocean will also influence the atmosphere. We aim to explore the influence of these parameters on possible biosignatures in future work. Hycean planets are of particular interest with regards to potential biosignature observations as their large size makes for easier observations compared to those of Earth-sized planets. Adding the biotic component of the model presented in this work into an abiotic Hycean model is another avenue of future work we hope to explore.

We focus here on methane since this potential biosignature can be readily detectable using current telescope technology (Thompson et al. 2022; Bell et al. 2023; Wogan et al. 2024; Lunine & Bahcall 2025). Methane has been detected in the atmospheres of K2-18b (Bézard et al. 2022; Madhusudhan et al. 2023b; Fernández-Rodríguez et al. 2026), and TOI-270d (Benneke et al. 2024; Holmberg & Madhusudhan 2024), both candidate Hycean exoplanets situated within the habitable zone of their stars. However, the detection of methane cannot automatically be taken as a biosignature as abundant methane is also detected in similarly-sized planets that are not thought to be habitable, such as the sub-Neptune planet LP791-18c which is not thought to have a solid surface (Roy et al. 2024). For terrestrial planets a detection of abundant methane would potentially constitute a stronger sign of life as there are no known abiotic pathways for rocky planets to acquire high quantities of methane (Wogan et al. 2020; Seager et al. 2025). However with their smaller size these planets are harder to observe and currently only those with close orbits to M-dwarf stars are accessible for atmospheric studies (TRAPPIST-1 JWST Community Initiative 2024). So far there has been no definitive detections of an atmosphere around a terrestrial planet (Lunine & Bahcall 2025). Both the robust detections of methane in the atmospheres of possible Hycean planets, and the potential strength of

methane as a biosignature for terrestrial planets motivates building models of methane producing biospheres that are minimally bound by assumptions based on Earth-based life.

In this work we aim to produce a generalised microbial cell model that can be added to abiotic models of exoplanets to determine the maximum accumulation of methane gas in the observable regions of the atmosphere of the planet as a by-product of life, given an assumed rate of  $H_2$  and  $CO_2$  outgassing. This will help guide observational searches by determining whether a predicted biosignature would accumulate in quantities high enough to be observable. The microbial cell model can also be used to calculate the necessary supply of  $H_2$  to the biosphere required to yield a certain abundance of methane for a specific exoplanet. By predicting the abiotic source of gases to a biosphere we can validate whether the predicted abundance of abiotic gases agrees with other measured properties of the planet, e.g. a predicted high  $H_2$  outgassing rate on a planet would imply a high rate of volcanic activity, which would leave other evidence in a planet’s atmosphere (Edmonds et al. 2022).

Any microbe cell model will unavoidably be specific to the given metabolism, however the approach to building the model cell taken here can be applied to nutrient limited chemosynthetic microbe cells with other metabolisms. How the biosignature accumulates in the environment will be specific to the metabolism itself and the planetary context (Thompson et al. 2022). Therefore this work presents a generalised microbial cell model for methane biosignature predictions, but the wider approach can be adopted for prediction of biosignature due to other nutrient limited chemosynthetic life.

Previous work by Nicholson et al. (2022) showed that for a simple nutrient-limited chemosynthetic microbial biosphere, the availability of the limiting substrate to the biosphere was significantly more important in determining the resulting biosignature gas in the atmosphere, than the specific biological parameters describing the microbial life, e.g. cell death rates and energy maintenance costs. Diffusion-limited substrate uptake was not included in Nicholson et al. (2022), and microbes in this model were able to consume nutrients down to concentrations of zero. Here we extend the model to include diffusion-limited substrate uptake with the aim of a more realistic and generalised microbe model that is more readily adaptable to different planetary scenarios. We find that including diffusion-limitation impacts the biosphere’s ability to draw down  $H_2$  when the biotic parameters describing the microbes change and thus in turn impacts the biosignature. By arguing that life will evolve to exploit limiting nutrients, and using studies determining the bounds of life as we know it, we propose a generalised microbial model for methane biosignature prediction modelling.

This paper is structured as follows. Section 2 outlines the model description and the parameter space explored in this work. We base our microbe model on lab measurements grounding it in known realistic biology, with model steps follow realistic microbe behaviours. In Section 3 we explore the impact of including diffusion-limited  $H_2$  uptake on the atmosphere biosignature. In Section 4 we argue that competition and evolution are likely to occur within alien biospheres allowing us to form predictions that limit the biological parameter space required to explore when formulating biosignature predictions for a chemosynthetic microbial biosphere. Finally, in Section 5 we present our conclusions.

## 2 METHODS

In this Section we briefly cover the planetary setup used in the following simulations and the biological parameters used to de-

scribe the model microbes. The physical parameters and planetary setup follow those used in [Nicholson et al. \(2022\)](#) and so a more complete description can be found there. The code used for the following simulations is also publicly available on github: <https://github.com/nicholsonae/biosignatures>.

## 2.1 Planet setup

For our planet setup we follow [Nicholson et al. \(2022\)](#) and assume an Earth-sized planet covered in a global ocean that orbits a sun-like star. As in [Nicholson et al. \(2022\)](#) the model planet’s atmosphere and ocean are represented in 0D. We assume an  $N_2$  dominated atmosphere and abundant  $H_2O$  for all reactions that require it. We track the movement of  $CO_2$ ,  $H_2$ , and  $CH_4$  through the system. We assume a constant atmospheric pressure,  $P_{atmo} = 1 \text{ atm}$ , and a constant total number of moles of gas comprising the atmosphere  $n_{atmo} = 1.73 \times 10^{20} \text{ mol}$  taking modern Earth values. The abiotic environment is updated with the inflows / losses of each traced gas in model time-steps representing years. Figure 1 shows a schematic of the model set up.

### 2.1.1 Atmosphere setup

We assume constant sources of  $H_2$ , and  $CO_2$  to the atmosphere in an approximation of volcanic outgassing. On Earth,  $H_2$  is lost from the upper atmosphere layers irreversibly to space via diffusion of  $H_2$ . Assuming a dry stratosphere ([Hunten 1973](#); [Walker 1977](#)), the rate of hydrogen loss is proportional to  $f(H_2) + 2f(CH_4)$  where  $f(H_2)$  and  $2f(CH_4)$  are the mixing ratios of  $H_2$  and  $CH_4$  respectively. We assume a constant rate of atmospheric hydrogen loss according to these ratios. In our model atmospheric  $CO_2$  removal occurs by removing a fixed percentage of the atmospheric  $CO_2$  each year. This acts as a highly simplified representation of silicate weathering. Abiotic  $CO_2$  removal from Earth’s atmosphere is far more complex than represented here ([West et al. 2005](#)), and the dependence of seafloor weathering on Earth’s climate is currently less understood ([Brady & Gíslason 1997](#)) and this process can act as either a sink or a source of  $CO_2$  to the ocean, adding an additional layer of complexity. As we are primarily interested in the biotic component of our system a simplified removal of  $CO_2$  is suitable.

We include no abiotic source of  $CH_4$  and on an Earth-like planet with no atmospheric  $O_2$ ,  $CH_4$  is long lived in the atmosphere and its breakdown occurs via photolysis at the top of the atmosphere. This is a complex process that is altitude dependant and has several steps, and so we [simplify](#) it here for our 0-D representation of a planet’s atmosphere and assume that methane breaks down according to  $CH_4 + 2H_2O \rightarrow CO_2 + 4H_2$  following [Kharecha et al. \(2005\)](#) and [Nicholson et al. \(2022\)](#). We assume that this  $CH_4$  breakdown occurs at a fixed rate proportional to the quantity of methane in the atmosphere.

The surface temperature of our model planet is  $CO_2$  and  $CH_4$  dependant. The parametrisation of temperature against atmospheric composition was generated using the Met Office Unified Model (UM) ([Boutle et al. 2017](#); [Eager-Nash et al. 2020](#)) through simulated snapshots of the planet’s temperature for different levels of  $CO_2$  and  $CH_4$  in the atmosphere. To generate these snapshots the UM is set up as described in [Eager-Nash et al. \(2023\)](#), assuming a 1 billion year old host star of type G and a planet radius of  $6051.3 \times 10^3 \text{ m}$ . Atmospheric configurations are then run to equilibrium for different atmospheric quantities of  $CH_4$  and  $CO_2$  and these snapshots are then interpolated into a 2D grid which informs the model planet’s temperature based

**Table 1.** Parameters for the abiotic influx and outflux of atmospheric  $CO_2$ ,  $H_2$ , and  $CH_4$ , where  $T(X)$  is the total number of moles of molecule  $X$  in the atmosphere.

Chemical	Influx ( $yr^{-1}$ )	Outflux ( $yr^{-1}$ )
$CO_2$	$10^{15}$	$0.001 \times T(CO_2)$
$H_2$	$10^{13}$	$0.001 \times (T(H_2) + 2T(CH_4))$
$CH_4$	0	$0.001 \times T(CH_4)$

on the atmospheric composition. For full details see [Nicholson et al. \(2022\)](#); [Eager-Nash et al. \(2023\)](#).

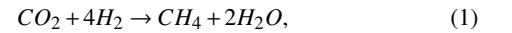
Table 1 shows the abiotic influxes and outfluxes of  $H_2$ ,  $CO_2$ , and  $CH_4$  to the planet atmosphere used for all of the following simulations. Abiotic influxes are kept fixed throughout simulations. We model the outgassing and abiotic removal of  $H_2$  and  $CO_2$  in an idealised way with values chosen to ensure a habitable surface suitable for seeding with microbes. To form biosignature predictions for a particular planet these parameters would need to be bespoke for the planet in question as factors such as the mass of the planet, and the properties of the host star will affect the rate of  $H_2$  loss from a planet’s atmosphere ([Hunten & Donahue 1976](#); [Miller-Ricci et al. 2009](#); [Savanov & Shematovich 2021](#)).

### 2.1.2 Ocean-atmosphere gas exchange

We assume that the only source of  $CO_2$  and  $H_2$  to the ocean is from the atmosphere. Gases in the atmosphere dissolve into the ocean and become available to the biosphere, and biotically produced methane (the only source of methane to the system) is exchanged between the ocean and the atmosphere. We calculate the molecular transfer of gases between the ocean and atmosphere following the stagnant boundary layer model ([Liss & Slater 1974](#)) where the exchange of gases depends on the concentration gradient through a thin film of water on the top of the ocean (full details can be found in Section A1).

## 2.2 Microbe model

We model a single-species single-celled chemosynthetic microbial biosphere, based on the *Methanosarcina barkeri* species, where microbes generate energy from the metabolism via



where the energy obtained from this reaction is given by the Gibbs free energy expressed as

$$\Delta G = \Delta G^0 + RT \log(Q). \quad (2)$$

$\Delta G^0$  is the free energy change of the reaction under standard conditions and we use  $\Delta G^0 = (-253 + 0.41 T) \text{ kJ mol}^{-1}$  following [Kral et al. \(1998\)](#),  $R$  is the universal gas constant ( $0.008314 \text{ kJ mol}^{-1} \text{ K}^{-1}$ ),  $T$  is the temperature in kelvin. For  $\Delta G_{CH_4}$  - the energy required to synthesise 1 mol of  $CH_4$  -  $Q$  is given by

$$Q = \frac{[CH_4]_{aq}^* \cdot a(H_2O)^2}{[CO_2]_{aq}^* \cdot ([H_2]_{aq}^*)^4}. \quad (3)$$

where  $[i]_{aq}^* = \frac{[i]_{aq}}{\alpha(i)}$  is the dissolved concentration of species  $i$  divided by its Henry’s law coefficient (its solubility). The values of  $\alpha(H_2)$ ,

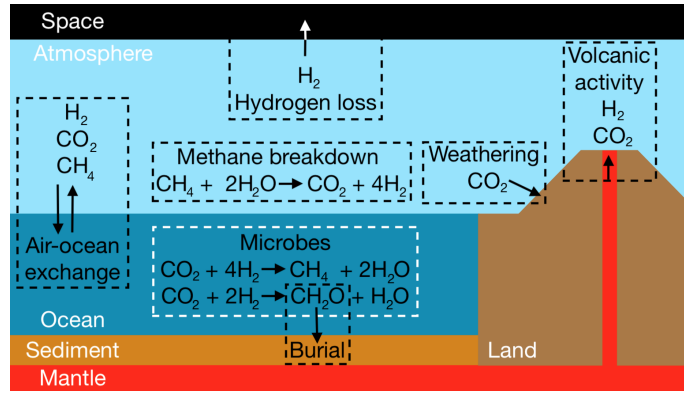
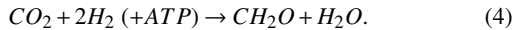


**Figure 1.** A schematic showing the key abiotic (black dashed boxes) and biotic (white dashed box) processes occurring in the model (reproduced from Nicholson et al. 2022).

$\alpha(\text{CO}_2)$ , and  $\alpha(\text{CH}_4)$  can be found in Table A1 and  $\alpha(\text{H}_2\text{O})$  is assumed to be 1 (Kharecha et al. 2005). We will explore two scenarios, one where  $\Delta G$  is given by Equation 2 and another where we fix  $\Delta G$  to be a constant value.

Our model microbes build their biomass following



We use  $\text{CH}_2\text{O}$  as a proxy for the microbes' biomass. We base the default microbe parameters around those determined in lab experiments for *Methanosarcina barkeri*, which gives us a baseline for modelling a realistic life-form. We can then change various parameters describing the microbes to test how changing these parameters change the microbes' impact on their environment.

In Nicholson et al. (2022) we included a parameter for the ATP maintenance cost of the microbes. Here we remove this parameter and instead vary the energy cost for biosynthesis. We can represent the energetic cost of microbes equivalently by either including a separate ATP maintenance cost, or by having a higher biosynthesis cost. Provided the overall energetic cost per mole of biomass is the same, whether the energy a microbe generates is for maintenance costs or biosynthesis costs is irrelevant and will produce the same amount of  $\text{CH}_4$ . See Appendix A2 for further discussion.

The microbe cell parameters that we vary are the cell radius (we assume cells to be spherical), the rate at which cells die, and the energy cost of synthesising 1 mole of biomass. We also have to include the energy cost to build biomass and generate ATP. We fix the biomass density of cells. We calculate the default values of these parameters based on data from lab experiments on microbes. Overall microbe cell mortality rates have been measured to be between  $0.01 - 0.03 \text{ h}^{-1}$  in aquatic environments (Servais et al. 1985) and so we use  $0.02 \text{ h}^{-1}$  as our default value here. A full list of the microbe parameters can be found in Table 2. Some of the parameters are taken directly from lab measurements and some we have adapted to use in our model. For full details on how the default values in Table 2 are calculated, see Appendix A3

### 2.2.1 Diffusion-limited substrate uptake

At steady state the flux of a substrate  $F$  ( $\text{mol s}^{-1}$ ), through the surface of a spherical cell of radius  $r$  ( $\text{m}$ ), is given by:

$$F = 4\pi r D S_\infty, \quad (5)$$

where  $D$  is the diffusion coefficient ( $\text{m}^2 \text{ s}^{-1}$ ) for the substrate and  $S_\infty$  is the concentration of the substrate ( $\text{mol m}^{-3}$ ) far from the cell wall

(Berg & Purcell 1977). Equation 5 makes the assumption that the cell is a perfect sink for the substrate molecules, i.e. a cell completely absorbs all molecules that reach its surface. Equation 5 therefore is a theoretical maximum diffusion-limited substrate uptake rate.

Armstrong (2008) follow Pasciak & Gavis (1974, 1975) in deriving the theoretical maximum diffusion-limited substrate uptake flux across a cell membrane. This uptake rate,  $F_D(r)$ , depends on distance from the centre of the cell,  $r$ , and is given by

$$F(r) = 4\pi D r^2 \frac{\partial S}{\partial r}, \quad (6)$$

where  $S_r$  is the substrate concentration at a distance  $r$  from the centre of the cell.

$$\int_{S_0}^{S_\infty} \partial S(r) = \frac{F(r_0)}{4\pi D} \int_{r_0}^{\infty} r^{-2} \partial r, \quad (7)$$

equates to

$$[S_\infty - S_0] = \frac{F(r_0)}{4\pi D} r_0^{-1}, \quad (8)$$

which can be rearranged to give

$$F(r_0) = 4\pi D r_0 [S_\infty - S_0]. \quad (9)$$

We then make the assumption that  $S_0 = 0$ , i.e. the cell absorbs all molecules of the substrate that reach its surface. Thus, we reach Equation 5 as our theoretical upper limit to diffusion limited substrate uptake by our microbes. While this is an upper limit, our model neglects other strategies microbes have evolved to uptake substrates such as moving to areas of higher substrate concentration and changing body shape to maximise surface area against the volume ratios, (e.g. growing appendages or movement (Pavlova et al. 2022)). We choose here to model a spherical cell to simplify both modelling diffusion into the cell and to enable changing the cell size with a single parameter - its radius. The effects of non-spherical cell shapes can be included in Equation 5 by multiplying by a dimensionless shape coefficient (see Armstrong 2008; Pasciak & Gavis 1975; Pahlow et al. 1997). As our aim here is to consider a qualitative study of an idealised and general model, and not to generate specific quantitative predictions, we focus on spherical cells. Including the impact of motion involves the more complex Sherwood number (see Armstrong 2008; Karp-Boss et al. 1996), which we retain for future work. As we are using an Archean Earth-like setup,  $\text{H}_2$  is the limiting substrate to the microbes and so their growth is limited by its availability. We use a diffusion coefficient for  $\text{H}_2$  of  $D_{\text{H}_2} \approx 4.3 \times 10^{-9} \text{ m}^2 \text{ s}^{-1}$  (Wang et al. 2023) to calculate the maximum  $\text{H}_2$  uptake of a microbe, and then

**Table 2.** Default biological parameters used for our model microbes. These values come from lab based measurements of the *Methanosarcina barkeri*, a single-celled methane producing archaea. Values labelled \* are taken from (Lynch et al. 2019). Values labelled † are based on results from Servais et al. (1985).

Cell parameter	Default values	Sensitivity tests
radius	$r_0 = 10^{-6} m$ *	$0.1r_0, 0.5r_0, 0.75r_0, r_0, 1.25r_0, 1.5r_0$
death rate	$d_0 = 0.02 h^{-1}$ †	$0.0, 0.005, 0.02, 0.04, 0.07, 0.1$
biomass density	$b_0 = 3530 mol_{CH_2O}/m^3$ *	
$\Delta G_{CH_2O}$	$m_0 = 97.5 kJ mol_{CH_2O}^{-1}$ *	$0.5m_0, m_0, 1.5m_0, 2m_0, 3m_0, 5m_0, 10m_0, 20m_0$

the  $CO_2$  uptake is calculated depending on how the  $H_2$  is ‘allocated’ by the microbe to either energy generation or biomass generation (Section 2.2.2). Note that for a different type of planet, e.g. a Hycean planet with a hydrogen-dominated atmosphere,  $CO_2$  would instead be the limiting substrate to microbe growth, and so the same approach could be taken but for determining the  $CO_2$  availability to the microbes instead of the  $H_2$  availability.

### 2.2.2 Calculating cell $H_2$ allocation

Microbes must obtain energy via Equation 1 which utilises  $H_2$ , and also use  $H_2$  to build biomass following Equation 4. The ratio at which  $H_2$  is ‘assigned’ to either biomass or energy generation depends on the energy obtained from the microbes’ metabolism, Equation 1. The energy generated per 1 mole of  $CH_4$  metabolised via Equation 1 is given by  $\Delta G_{CH_4}$ , Equation 2. Therefore the energy obtained per mole of  $H_2$  is given by

$$\frac{\Delta G_{CH_4}}{4}. \quad (10)$$

We use values from Lynch et al. (2019) for the energy required to synthesise 1 mole of  $ATP$ , and the number of moles of  $ATP$  required to build 1 mole of  $CH_2O$  to calculate the total energy required to build 1 mole of  $CH_2O$  (see Appendix A3 for further details).

The energy required to metabolise 2 moles of  $H_2$  into 1 mole of biomass ( $CH_2O$ ) is given by

$$\Delta G_{ATP} \times ATP_{CH_2O} = \Delta G_{CH_2O} \quad (11)$$

where  $\Delta G_{ATP}$  is the energy required to synthesise a mole of  $ATP$  and  $ATP_{CH_2O}$  is the number of moles of  $ATP$  required to synthesise 1 mole of  $CH_2O$ . Therefore the number of moles of  $H_2$  required for energy generation in order to build 1 mole of  $CH_2O$  is

$$\frac{4 \Delta G_{CH_2O}}{\Delta G_{CH_4}} \quad (12)$$

As we require 2 moles of  $H_2$  to build 1 mole of  $CH_2O$  then the number of moles of  $H_2$  required for energy generation per mole of  $H_2$  used for biomass synthesis is given by

$$H_2^{biomass} : H_2^{energy} = 1 : \frac{2 \Delta G_{CH_2O}}{\Delta G_{CH_4}}. \quad (13)$$

The maximum  $H_2$  uptake by a cell is given by the diffusion-limited rate (Equation 5), and microbes will then assign  $H_2$  to either energy generation or biomass synthesis according Equation 13.

## 2.3 Model structure

Microbial growth rates are often given in terms of units of an hour (e.g. Weissman et al. 2021), whereas climate simulations tend to sta-

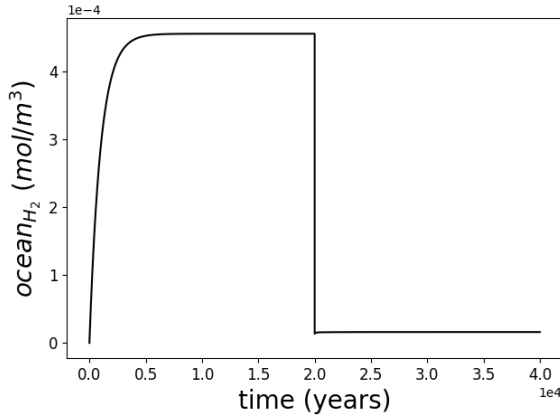
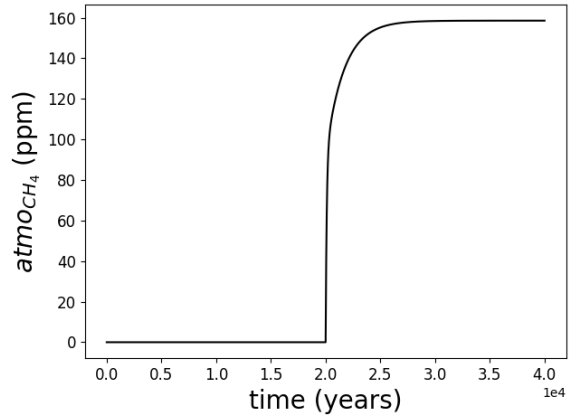
bilise over the course of years or decades to changes in atmospheric composition (Eager-Nash et al. 2023), therefore the abiotic environment is updated on timesteps representing years and the microbe biosphere is updated on timesteps representing hours. The microbe population is recorded in terms of the total biomass of the biosphere, and  $ATP$  available to the biosphere. The population of the biosphere can be calculated by dividing the total biomass of the biosphere by the biomass contained within one microbe cell.

Once the model is initialised, it is run for 20,000 years before seeding with life to allow the atmosphere and ocean to reach equilibrium. Life is then seeded at  $t = 20,000$  years and the model is run for a further 20,000 years to allow the system to reach a steady state after the introduction of life (which happens by roughly 10,000 years after the appearance of life (see Figure 2b)). The atmospheric and oceanic abundances of  $H_2$ ,  $CO_2$ , and  $CH_4$  are recorded along with the microbe population. See Appendix A4 for further details on the timesteps of the model. To test the sensitivity of the biological parameters on our results we change one biological parameter at a time, keeping the others fixed to the default ones listed in the ‘Default values’ column of Table 2.

## 3 RESULTS

When life is introduced to the planet the concentration of  $H_2$  in the ocean rapidly drops before stabilising at a low concentration due to the microbes’ consumption of  $H_2$ , and the level of  $CH_4$  in the atmosphere rises rapidly. Figure 2a and 2b shows the concentration of  $H_2$  in the ocean, and the abundance of  $CH_4$  in the atmosphere, respectively, over time. In each case, the introduction of life at  $t = 20,000$  years is clearly seen. The concentration at which ocean  $H_2$  stabilises depends on the rate at which microbes require to uptake  $H_2$  to maintain a stable population. As described in Section 2.2.1 the flow of molecules into the cell depends on the concentration of the substrate in the ocean. A stable microbial population is only achieved when the birth rate (which depends on the uptake rate of  $H_2$  by the microbe) matches the death rate of the microbes (which is a set parameter, see Table 2). Therefore the concentration of  $H_2$  in the ocean stabilises at a ‘limiting concentration’. Below this limiting concentration the population of the microbes will drop, leading to fewer microbes removing  $H_2$  from the ocean and thus allowing the concentration of  $H_2$  to rise via diffusion from the atmosphere, and above the limiting concentration the population of the microbes will increase and thus  $H_2$  will be removed more rapidly from the ocean lowering its concentration. In this way the concentration of  $H_2$  in the ocean is regulated by the biosphere (see Nicholson et al. 2022, for further details).

The rest of this section presents results on how changing the cell

(a) Concentration of  $H_2$  in the ocean over time.(b) Level of  $CH_4$  in the atmosphere against time.

**Figure 2.** Panels showing the concentration of  $H_2$  in the ocean,  $ocean_{H_2}$  and the level of methane in the atmosphere  $atmo_{CH_4}$  over time. Life is introduced to the system at  $t = 20,000$  years.

parameters of cell radius, cell death rate, and the energy cost of biomass synthesis impact the biotic  $CH_4$  output for scenarios where cell uptake of  $H_2$  is limited by diffusion, as given by Equation 5. In Section 3.1 we discuss the impact of changing the cell radius or cell death rate, and then in Section 3.2 we discuss how changing the energetic cost of biomass ( $CH_2O$ ) synthesis changes the model dynamics.

### 3.1 Changing the cell radius or cell death rate

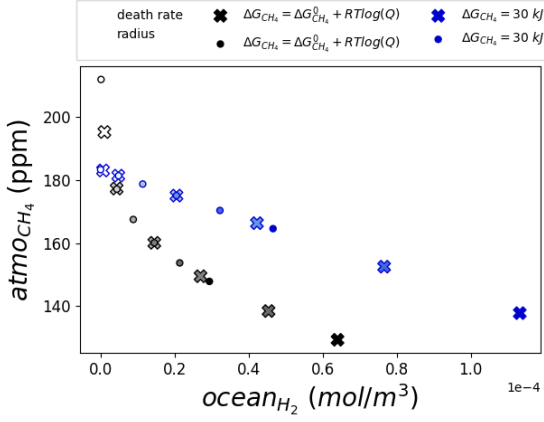
Figure 3a shows level of methane in the atmosphere,  $atmo_{CH_4}$  against the concentration of hydrogen in the ocean  $ocean_{H_2}$  for simulations with differing cell death rates (shown with  $\times$  markers) and radii (shown with  $\circ$  markers) as listed in Table 2. There are two energy scenarios shown, those where  $\Delta G_{CH_4}$  is given by Equation 2, shown in black, and data where  $\Delta G_{CH_4} = 30$  kJ, shown in blue. The colour saturation of each point correlates with the parameter value, i.e. a darker filled circle indicates a large cell radius, and a lighter filled circle indicates a small cell radius. Each data-point represents a microbial biosphere with fixed cell parameters throughout the simulation, and for experiments of different cell death rates, the cell radius is set to the default value in Table 2, and similarly for experiments of different cell radii, the cell death rate is set to the default value in Table 2.

Figure 3a shows an overall trend in the data that as we increase either the cell size, or the cell death rate (indicated by a higher marker colour saturation) the level of  $H_2$  in the ocean increases, and the level of methane in the atmosphere decreases. The correlation between  $atmo_{CH_4}$  and  $ocean_{H_2}$  is linear where  $\Delta G_{CH_4}$  is fixed (blue data), and non linear when  $\Delta G_{CH_4}$  is given by Equation 2. Figure 3b shows the same data but this time for the level of methane in the atmosphere against the rate of hydrogen inflow to the ocean. In Figure 3b we can see that  $atmo_{CH_4}$  increases linearly with  $H_2$  inflow to the ocean when  $\Delta G_{CH_4}$  is fixed (blue data). This agrees with previous findings of Nicholson et al. (2022), i.e. that the strength of a biosignature linearly increases with an increase of the availability of the limiting nutrient to the biosphere. The inflow of  $H_2$  to the ocean scales with the concentration of  $H_2$  in the ocean (transfer of  $H_2$  from the atmosphere to the ocean increases as  $ocean_{H_2}$  decreases, see Appendix A1 for more details).

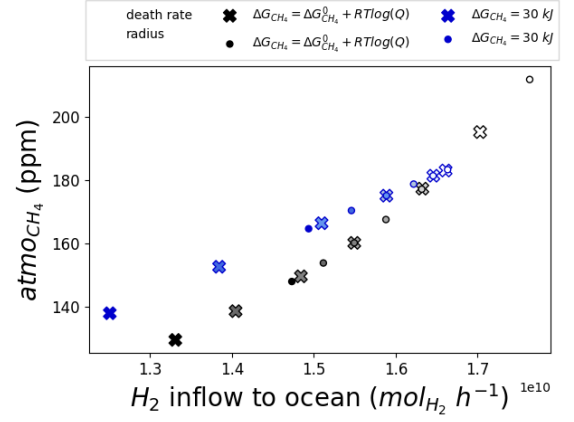
For a stable population the birth rate of cells must match the

death rate, meaning cells must accumulate sufficient biomass via Equation 4 to build a new cell before dying. Given the same cell death rate, a smaller cell will need to build biomass at a slower rate to achieve this compared to a larger cell. This leads to smaller cells having lower  $H_2$  requirements per hour than larger cells. The  $H_2$  cell uptake rate depends on  $ocean_{H_2}$  (see Equation 5) with faster  $H_2$  uptake rates occurring for higher values of  $ocean_{H_2}$ . Therefore  $ocean_{H_2}$  will be maintained at a lower level for a biosphere consisting of smaller cells due to the lower uptake rate of  $H_2$  that is required for a stable population. If  $ocean_{H_2}$  drops below a level that can sustain a stable population, microbes will begin to starve and thereby as fewer microbes are removing  $H_2$  from the ocean, the  $ocean_{H_2}$  increases. If  $ocean_{H_2}$  is higher than the level required for a stable population, microbes will reproduce a rate above the cell death rate, leading to a higher population and thus a reduction in  $ocean_{H_2}$ . This feedback leads to biotic regulation of the concentration of  $H_2$  in the ocean. Reducing the death rate of cells corresponds to a lower  $ocean_{H_2}$  for a similar reason. Longer lived cells do not need to build biomass as rapidly as shorter lived cells and so have a lower  $H_2$  uptake requirement and thus  $ocean_{H_2}$  is maintained at a lower level.

The level of methane in the atmosphere depends both on the availability of hydrogen to the biosphere, and the energy available to the biosphere when synthesising  $H_2$  to  $CH_4$  which in turn depends on the concentrations of  $H_2$ ,  $CH_4$  and  $CO_2$  in the ocean, see Equations 2 and 3. Figure 4 shows the population of the biosphere (4a), the  $H_2$  uptake rate per microbe cell (4b), the  $H_2$  allocation to either energy generation or biomass (4c), and the biomass of the biosphere (4d) against the the concentration of  $H_2$  in the ocean for both cases with a fixed  $\Delta G_{CH_4}$  (shown in blue), and where  $\Delta G_{CH_4}$  varies as given by Equation 2. As before the colour saturation of each point correlates with the parameter value, with darker saturations indicating higher parameter values. From Figures 4a and 4b we find that increasing either the cell death rate or cell size leads to a decrease in the biosphere's population, and increase in individual cell  $H_2$  uptake (as well as the increase in  $ocean_{H_2}$  already discussed). Figures 3a 3b show that an increase in  $ocean_{H_2}$  correlates with a decrease in the inflow of  $H_2$  from the atmosphere to the ocean, thus decreasing the availability of  $H_2$  to the biosphere. The individual microbe's  $H_2$  uptake needs set the concentration of  $H_2$  in the ocean as discussed above and this uptake rate increases linearly with  $ocean_{H_2}$  as we increase the cell death rate, and increases at a faster rate when increasing the cell size.

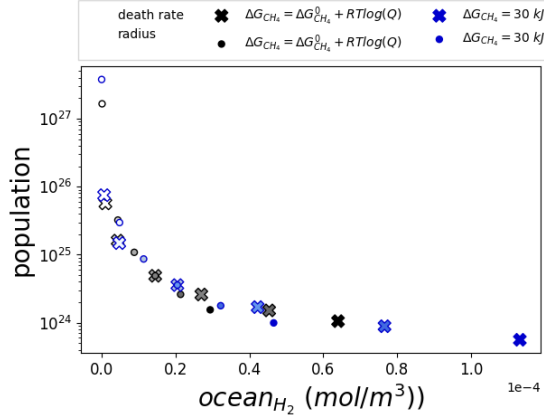


(a) Level of  $CH_4$  in the atmosphere against the concentration of  $H_2$  in the ocean.

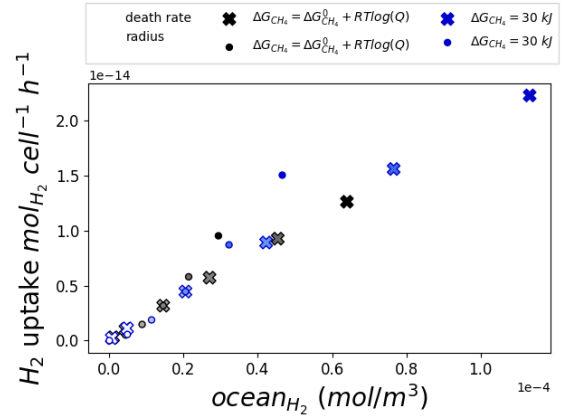


(b) Level of  $CH_4$  in the atmosphere against the the rate of  $H_2$  inflow into the ocean.

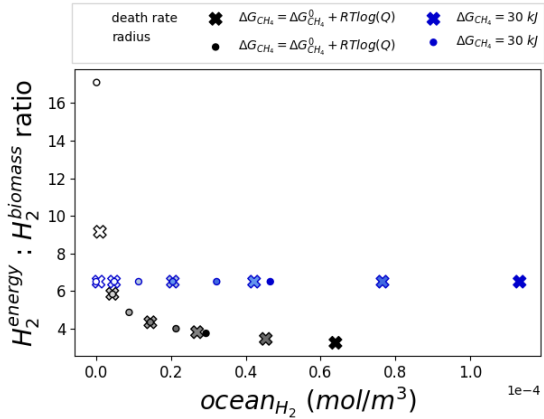
**Figure 3.** Panels showing data from experiments with different cell death rates, marked with an  $\times$ , and different cell radii, marked with an  $\circ$ , for experiments where  $\Delta_{CH_4}$  is given by Equation 2, shown in black, and for experiments with fixed  $\Delta_{CH_4} = 30 \text{ kJ}$ , shown in blue. Marker colour saturation indicates the parameter value for the  $CH_2O$  synthesis cost with a darker marker indicating a higher cost of  $CH_2O$  synthesis.



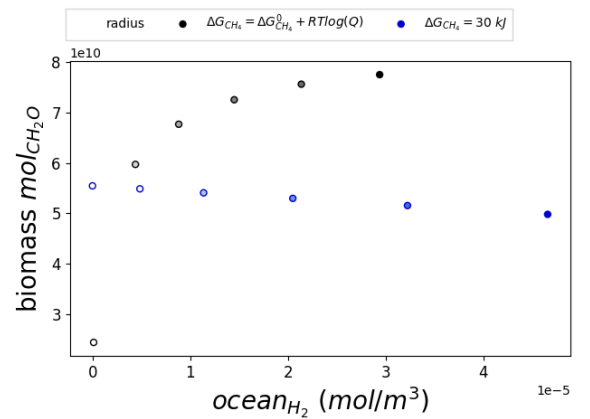
(a) Total population of the biosphere as a function of the concentration of  $H_2$  in the ocean.



(b) Rate of  $H_2$  uptake per microbe cell as a function of the concentration of  $H_2$  in the ocean.



(c) Ratio of  $H_2$  allocated to energy generation as a function of the biomass synthesis against the concentration of  $H_2$  in the ocean.



(d) Total biomass of biosphere as a function of the concentration of  $H_2$  in the ocean.

**Figure 4.** Panels showing data from experiments with different cell death rates, marked with an  $\times$ , and different cell radii, marked with an  $\circ$ , for experiments where  $\Delta_{CH_4}$  is given by Equation 2, shown in black, and for experiments with fixed  $\Delta_{CH_4} = 30 \text{ kJ}$ , shown in blue. Marker colour saturation indicates the parameter value for the  $CH_2O$  synthesis cost with a darker marker indicating a higher cost of  $CH_2O$  synthesis.

The radius of the cell also impacts the  $H_2$  uptake rate (see Equation 5), with faster uptake for higher cell radii, causing this difference in behaviour. Therefore increasing cell death rate or cell size reduces the total availability of  $H_2$  to the biosphere leading to a decrease in the level of methane in the atmosphere.

Figure 4c shows the ratio of  $H_2$  used for energy generation as opposed to biomass building as a function of ocean  $H_2$ . When  $\Delta G_{CH_4}$  is fixed (blue data) this ratio is constant and this leads to the linear relationship between  $atmo_{CH_4}$  and  $ocean_{H_2} / H_2$  inflow to the ocean seen in Figure 3. However when  $\Delta G_{CH_4}$  is given by Equation 2, it increases as  $ocean_{H_2}$  increases and thus the ratio of  $H_2$  going to energy against the biomass decreases with increasing  $ocean_{H_2}$ . As the microbes can achieve more energy per mole of  $CH_4$  synthesised they can more efficiently use  $H_2$  to build biomass. For very low concentrations of  $H_2$  in the ocean the energy yield for  $CH_4$  synthesis is low and so microbes must use more  $H_2$  for energy synthesis which increases the biosignature.

Figure 4d shows the biomass of the biosphere as a function of  $ocean_{H_2}$  for the cell radius experiments. When changing the cell death rate the biomass within a cell is unchanged and so the biomass scales with population (Figure 4a). However, when we change the cell radius, the relationship between the population and the biomass of the biosphere changes. Figure 4d shows that where  $\Delta G_{CH_4}$  is fixed the biomass drops as we increase the cell size (indicated by darker circles) and  $ocean_{H_2}$  decreases albeit slower than the population declines. The increased cell size leads to the biomass of the biosphere declining much more slowly than the population declines when  $\Delta G_{CH_4}$  is fixed. However, when  $\Delta G_{CH_4}$  is given by Equation 2, as the cell size increases, the biomass of the biosphere increases despite the population decreasing. The increased energy obtained by microbes per mole of  $CH_4$  synthesised allows for more  $H_2$  to be used for biomass synthesis and thus a lower biosignature and a higher amount of biomass than for fixed  $\Delta G_{CH_4}$  scenarios.

### 3.2 Changing the biomass synthesis cost

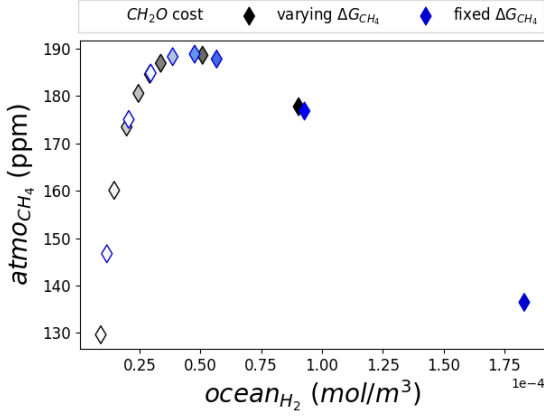
Changing the energy cost of synthesising 1 mole of  $CH_2O$  impacts the model behaviour differently to changing the cell size or cell death rate. Figure 5a shows  $atmo_{CH_4}$  against  $ocean_{H_2}$  for a range of experiments with different  $CH_2O$  synthesis costs (see Table 2). As before darker marker saturation correlates with a higher  $CH_2O$  cost. Figure 5a shows an initial increase in  $atmo_{CH_4}$  with increasing  $ocean_{H_2}$  as the  $CH_2O$  cost increases, before decreasing after a peak. Figure 5b shows  $atmo_{CH_4}$  against the inflow of  $H_2$  to the ocean. We see again a peak in  $atmo_{CH_4}$  however as we increase the  $CH_2O$  cost (indicated by darker markers) we see initially that  $atmo_{CH_4}$  increases with an increased inflow of  $H_2$  to the ocean, but that after the  $atmo_{CH_4}$  peak the  $H_2$  inflow to the ocean begins to decrease with increasing  $CH_2O$  cost. This shows that there are two distinct  $atmo_{CH_4}$  scenarios that can result from the same  $H_2$  inflow rate to the ocean, this is due to the recycling of methane in the atmosphere, as described in Section 2 which impacts the level of  $H_2$  in the atmosphere which also determines the rate of inflow of  $H_2$  to the ocean. This leads to the same rate of  $H_2$  inflow to the ocean being possible for two different concentrations of  $H_2$  in the ocean. See Appendix A5 for experiments where methane recycling in the atmosphere is omitted.

Figure 5c shows the biosphere population as a function of  $ocean_{H_2}$  for changing  $CH_2O$  synthesis costs. As the biomass contained within a cell is constant throughout the  $CH_2O$  synthesis cost experiments the biomass of the biosphere will scale with the population. As with increasing either the cell radius or cell death rate, Figure 5c shows that increasing the  $CH_2O$  cost decreases the population while  $ocean_{H_2}$

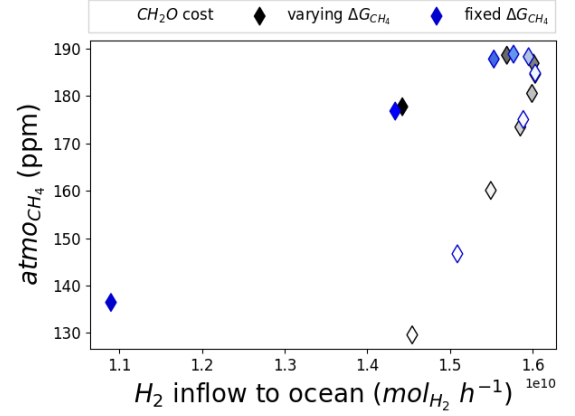
increases. The cell death rate is the same for all experiments and so therefore is the reproduction rate, however for microbes with higher  $CH_2O$  costs, microbes require a faster rate of  $H_2$  uptake to maintain a stable population and therefore require higher concentrations of  $H_2$  in the ocean. With more  $H_2$  needed for energy generation as the cost of  $CH_2O$  synthesis increases only lower populations can be supported by the environment. Figure 5d shows the ratio of  $H_2$  used for energy generation as a function of biomass synthesis and shows a linear relationship with increasing  $ocean_{H_2}$ . The  $H_2$  uptake of each microbe cell also scales linearly with  $ocean_{H_2}$  (see the death rate data in Figure 5d). Initially, the drop in population does not offset the increased  $CH_4$  output per microbe due to the increasing energy costs of synthesising biomass, and so  $atmo_{CH_4}$  initially increases. At  $ocean_{H_2} \approx 0.5 \text{ mol/m}^3$  the balance between the drop in population and the increased  $CH_4$  output per microbe changes and  $atmo_{CH_4}$  begins to decrease with increasing  $ocean_{H_2}$  as the cost of  $CH_2O$  is further increased.

## 4 FORMULATING PLAUSIBLE BIOSIGNATURE PREDICTIONS

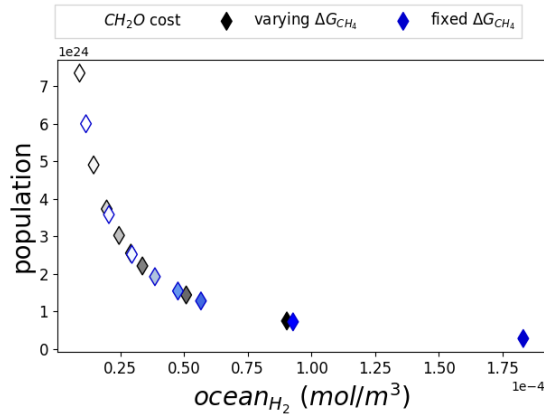
In Section 3 we analysed how changing the biological parameters governing the behaviour of model microbes, namely cell death rate, cell size, and biomass energy synthesis costs, impacts the the total population of the biosphere, the quantity of biologically produced  $CH_4$ , and the concentration of  $H_2$  maintained in the ocean by the biosphere. Figure 3a shows that increasing any of the cell parameters of cell size, cell death rate or the energy cost of biomass synthesis act to increase the concentration of  $H_2$  in the ocean, as increasing these parameters necessitates a faster rate of  $H_2$  uptake per microbe for the biosphere to maintain a steady population. On Earth competition for resources is a crucial driver of adaptation and evolution and most definitions of life include the ability to adapt via natural selection (Vitas & Dobovišek 2019), therefore it is a process we expect to be present in an alien biosphere - the organism most able to exploit a limiting resource will outcompete other species / subspecies and come to dominate that ‘niche’ in the environment. Within our model this competition would lead to the microbe able to draw  $H_2$  in the ocean down to the lowest concentrations outcompeting species than can only function at higher  $H_2$  concentrations in the ocean due to needing faster rates of  $H_2$  uptake. Therefore from our results, microbes that are smaller, longer lived, and with lower energy biomass synthesis costs will outcompete those which are shorter lived, larger, more dense, or have higher energy costs. For the parameters of cell size and cell death rate, smaller values lead not only to lower concentrations of  $H_2$  in the atmosphere but also higher levels of  $CH_4$  being produced by the biosphere and thus accumulating in the atmosphere. Therefore a microbial biosphere of longer lived, smaller cells would not only outcompete larger, shorter lived cells, but would also be easier for us to observe remotely. We can’t have an infinitely small cell, as life requires some minimum size and biomass to contain genetic information, a cell wall, energy storage, etc. Definitions of life also exclude it from being immortal, or at least the cells consisting of the organism from being immortal. Entropy dictates that cells will be required to spend energy on maintaining / replacing biomass. The smallest cells on Earth are heterotrophs, however when considering biosignatures we want an approximation for the primary producers of any alien biosphere. The smallest cell sizes for methanogenic life have been measured as having a length of  $0.6 \mu\text{m}$  and width of  $0.1 \mu\text{m}$  (Michal et al. 2018) which would correspond to a radius of  $\approx 0.2 \mu\text{m}$  for a spherical cell assuming the same volume. Ortega-Arzola et al.



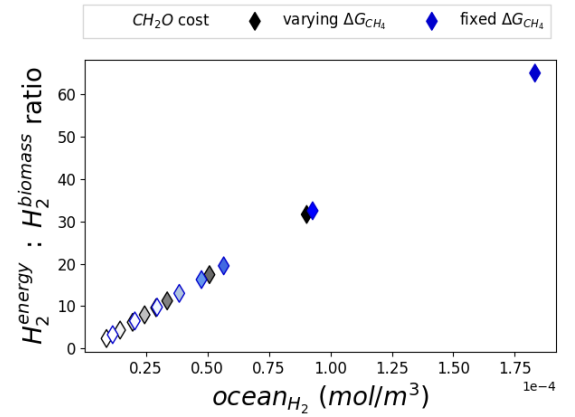
(a) Level of  $CH_4$  in the atmosphere as a function of the concentration of  $H_2$  in the ocean.



(b) Level of  $CH_4$  in the atmosphere as a function of the rate of  $H_2$  inflow into the ocean.



(c) Total population of the biosphere as a function of the concentration of  $H_2$  in the ocean.



(d) Ratio of  $H_2$  allocated to energy generation as a function of the biomass synthesis against the concentration of  $H_2$  in the ocean.

**Figure 5.** Panels showing data from experiments with different  $CH_2O$  synthesis costs for experiments where  $\Delta_{CH_4}$  is given by Equation 2, shown in black, and for fixed  $\Delta_{CH_4} = 30 \text{ kJ}$ , shown in blue. Marker colour saturation indicates the parameter value for the  $CH_2O$  synthesis cost with a darker marker indicating a higher cost of  $CH_2O$  synthesis.

(2024) investigates minimal energy costs for cell building and present a ‘minimal’ cell (Hutchison III et al. 2016; Breuer et al. 2019; Moger-Reischer et al. 2023). This minimal cell is able to replicate and fulfil all its metabolic needs and is smaller than any known free-living cell on Earth. As briefly discussed in Section 2.2.1 the effects of shape and motion on the uptake of nutrients by cells can be explored by including the relevant parameters to Equation 5 (see Armstrong 2008). These kinds of studies can be used to determine a reasonable estimate for the minimum size of a hypothetical alien cell to use in biosignature prediction models.

A lower bound for the death rate of microbe cells is hard to constrain even for microbes on Earth (Wu et al. 2024) as microbes can survive for months during periods of nutrient or water scarcity (Hobbie & Hobbie 2013; Leung et al. 2020; Mason-Jones et al. 2022), or for thousands of years in a dormant state while frozen in ice (Caro et al. 2025). However microbes in these latter scenarios only metabolise very slowly as they spend much of their time in stasis and so would be unlikely to produce observable biosignatures. Any life likely to leave an observable biosignature will be in an active, metabolising state. Measurements of ‘residual’ microbe cell death (e.g. cell death not due to predation) in marine ecosystems has been measured as being between  $0.002 - 0.02 \text{ h}^{-1}$  (Servais et al. 1985).

In a multi-species ecosystem grazing behaviour by heterotrophs may become important and additional mortality from grazing has been measured to be  $0 - 0.02 \text{ h}^{-1}$  for marine ecosystems (Servais et al. 1985).

The measured energy cost for biomass synthesis (which is typically recorded in units of moles of ATP required per mole of biomass in laboratory experiments) for microbes varies significantly. The work of Ortega-Arzola et al. (2024) aims to calculate a minimal energy cost for building a cell and includes a more realistic description of the components of a cell than presented here (where cells consist simply of ‘biomass’ represented by  $CH_2O$ ). Across 4 different cell types they find a very similar minimal energy cost of cell synthesis per gram which gives confidence that generalised models of cells can be applied in astrobiological settings. They note that there is little available thermodynamic data available for biopolymers and utilise group contribution methods to estimate energetic costs for biomass synthesis. Here, for methane biosignatures, we have identified that there is a peak in the  $CH_4$  produced by a biosphere when changing the biomass synthesis cost. For our goal of determining the maximum biosignature plausibly produced by a biosphere, we can identify where this peak  $CH_4$  output occurs for the microbe cells under the conditions predicted to be present on the exoplanet in question as this

peak depends both on the parameters chosen for the other biological parameters describing the microbes' cells, and on the physical environment.

The model discussed in this work can be used in two ways in astrobiology research. Firstly, given a modelled abiotic planet with estimations for abiotic parameters such as  $H_2$  outgassing, the generalised model can be used to form a maximum biosignature strength by inputting the plausible minimal estimations for cell size, a low cell death rate, and the energetic cost of biomass synthesis where the biosignature peaks (see Figure 5a). Alternatively the model can be used to calculate abiotic parameters of a planet where there has been a tentative detection of life. On a planet with life, life will act to 'erase' abiotic aspects of their environment. For example in the models discussed in this work, despite a high rate of  $H_2$  being supplied to the environment,  $H_2$  levels in the atmosphere and oceans are kept much lower due to life consuming  $H_2$ . If a planet with abundant methane was detected, this model can be used to calculate the minimum  $H_2$  influx required for a simple methanogen biosphere to produce the biosignature. This could help yield a prediction for e.g. how volcanically active the planet might be, and this could be compared with other observable evidence to corroborate or falsify this prediction (Edmonds et al. 2022).

While not the focus of this work, this model can also yield a prediction for the amount of biomass present to produce a potentially observed biosignature. This enables us to link predictions from our model with the biomass based model of determining biosignature plausibility developed by Seager et al. (2013) which use data from life on Earth to estimate whether the biomass required to produce a proposed biosignature is plausible.

## 5 CONCLUSIONS

In this work we have demonstrated that a simplified model of chemosynthetic microbial life, whose growth is limited by substrate availability, can be represented by a few key assumptions the cell metabolism, the cell size, the rate of cell death, and the energetic cost of biomass synthesis. We make the argument that we would expect evolution and competition for resources to be a feature of alien biospheres (and these processes are required for most definitions of life) and so we would expect alien life to evolve to exploit their environment to some limiting degree. In this model the limiting factor on microbe growth rate is  $H_2$  availability. We find that decreasing cell death rates, cell sizes and cell biomass densities all lead to lower concentrations of  $H_2$  in the ocean and also higher abundances of  $CH_4$  in the atmosphere, which in our model acts as our biosignature. Therefore, due to resource competition we would expect alien life to evolve to be smaller and longer lived. We can use studies investigating the smallest cell possible to inform our model. Constraining the cell death rate is less straightforward as e.g. the presence of high levels of UV radiation, or extreme temperatures will impact the rate of cell damage and death, as will the presence or absence of secondary consumers. When forming biosignature predictions, we can use measurements of microbe cell death rates both with and without the affects of grazing to inform our models e.g. Servais et al. (1985).

We would expect real alien biospheres to be vastly more complex than our simple model here, not only because alien biospheres are likely to consist of multiple species (Arthur & Nicholson 2017, 2022, 2023), some of whom consume the outputs of others, which will dramatically impact the biosignature. For example, secondary consumers that recycle the biomass of dead methane producing microbes increasing the methane signature in the atmosphere. The aim

of this work is to provide a baseline model for a microbial cell, where different metabolisms can be modelled and predictions for alien biospheres can start to be built where the model assumptions are clearly laid out and minimal in number.

Earth's biosphere is dominated by plant and microbial life (Bar-On et al. 2018) and these lifeforms are essential for more complex life such as mammals to evolve. Earth's microbial world has been likened to the 'life support system' of our biosphere due to the fundamental role it plays in shaping the surface of our planet (Cavicchioli et al. 2019). The majority of Earth's remotely observable biosignatures (Sterzik et al. 2012) are the products of either plant life, or microbial life, such as the 'red-edge', a sharp increase in albedo in wavelengths over  $700nm$  due to surface vegetation, and a large disequilibrium in the atmospheric abundances of methane and oxygen. Therefore constraining our possible parameter space for describing hypothetical alien plant or microbe life is vital for forming biosignature predictions for a range of alien biosphere scenarios. This does assume that an alien biosphere would similarly have a fundamental foundation of microbial life supporting any larger lifeforms as is the case for Earth's biosphere. In this work we have taken steps to develop a minimal cell model that can be used for biosignature predictions for nutrient-limited chemosynthetic life, and in future work plan to extend this approach to photosynthetic microbes and plants.

The goal of detecting and ultimately verifying the presence of life on a planet other than Earth requires extensive, multi-disciplinary effort, and simple, idealised, models informed by life on Earth, but minimally constrained by assumptions relevant to the specifics of Earth life, are required as part of this effort. Much more work is required, both in terms of increasing model complexity, exploring the impact of additional processes and feedbacks, for example, dynamics/circulations and atmospheric chemistry, and simplified approaches exploring the primary mechanisms ultimately controlling the observational signatures.

## ACKNOWLEDGEMENTS

This work was supported by a UKRI Future Leaders Fellowship and extension [grant numbers MR/T040866/1 & MR/Z000122/1]. This work was partly funded by the Leverhulme Trust through a research project grant [RPG-2020-82]. We'd like to thank the two anonymous reviewers for their helpful feedback in improving this manuscript.

## DATA AVAILABILITY

The code used to generate the data in this study can be found at: <https://github.com/nicholsonae/biosignatures>

## REFERENCES

- Armstrong R. A., 2008, *Deep Sea Research Part I: Oceanographic Research Papers*, 55, 1311
- Arthur R., Nicholson A., 2017, *Journal of theoretical biology*, 430, 177
- Arthur R., Nicholson A., 2022, *Journal of Theoretical Biology*, 533, 110940
- Arthur R., Nicholson A., 2023, *AstroBiology*, 23, 1238–
- Arthur R., Nicholson A. E., Mayne N. J., 2025, *MNRAS*, 541, 3664
- Bar-On Y. M., Phillips R., Milo R., 2018, *Proceedings of the National Academy of Sciences*, 115, 6506
- Bell T. J., et al., 2023, *Nature*, 623, 709
- Benneke B., et al., 2024, arXiv preprint arXiv:2403.03325
- Berg H., Purcell E., 1977, *Biophysical Journal*, 20, 193
- Bézard B., Charnay B., Blain D., 2022, *Nature Astronomy*, 6, 537

- Boutle I. A., Mayne N. J., Drummond B., Manners J., Goyal J., Lambert H. F., Acreman D. M., Earnshaw P. D., 2017, *Astronomy & Astrophysics*, 601, 13
- Brady P. V., Gíslason S. R., 1997, *Geochimica et Cosmochimica Acta*, 61, 965
- Breuer M., et al., 2019, *Elife*, 8, e36842
- Broecker W., Beng Z., Observatory L.-D. G., 1982, Tracers in the Sea. A Publication of the Lamont-Doherty geological observator, Lamont-Doherty Geological Observatory, Columbia University, <https://books.google.co.uk/books?id=uFq20AEACAAJ>
- Bruggeman J., Bolding K., 2014, *Environmental modelling & software*, 61, 249
- Caro T. A., McFarlin J. M., Maloney A. E., Jech S. D., Barker A. J., Douglas T. A., Barbato R. A., Kopf S. H., 2025, *Journal of Geophysical Research: Biogeosciences*, 130, e2025JG008759
- Catling D. C., et al., 2018, *Astrobiology*, 18:6
- Cavicchioli R., et al., 2019, *Nature Reviews Microbiology*, 17, 569
- Cloutier R., et al., 2019, *Astronomy & Astrophysics*, 621, A49
- Eager-Nash J. K., et al., 2020, *Astronomy & Astrophysics*, 639, A99
- Eager-Nash J. K., et al., 2023, *Journal of Geophysical Research: Atmospheres*, 128, e2022JD037544
- Edmonds M., Mason E., Hogg O., 2022, *Annual Review of Earth and Planetary Sciences*, 50, 79
- Feist A. M., Scholten J. C., Palsson B. Ø., Brockman F. J., Ideker T., 2006, *Molecular systems biology*, 2, 2006
- Fernández-Rodríguez G., et al., 2026, *Astronomy & Astrophysics*
- Foreman-Mackey D., Montet B. T., Hogg D. W., Morton T. D., Wang D., Schölkopf B., 2015, *The Astrophysical Journal*, 806, 215
- Fujii Y., et al., 2018, *Astrobiology*, 18, 739
- Hill M. L., Bott K., Dalba P. A., Fetherolf T., Kane S. R., Kopparapu R., Li Z., Ostberg C., 2023, *The Astronomical Journal*, 165, 34
- Hobbie J. E., Hobbie E. A., 2013, *Frontiers in microbiology*, 4, 324
- Holmberg M., Madhusudhan N., 2024, *Astronomy & Astrophysics*, 683, L2
- Hunten D., 1973, *Journal of Atmospheric Science*, 30, 1481
- Hunten D., Donahue T. M., 1976, In: *Annual review of earth and planetary sciences*. Volume 4.(A76-37259 18-91) Palo Alto, Calif., Annual Reviews, Inc., 1976, p. 265-292., 4, 265
- Hutchison III C. A., et al., 2016, *Science*, 351, aad6253
- Janssen P. H., Schuhmann A., Bak F., Liesack W., 1996, *Arch. Microbiology*, 166, 184
- Karp-Boss L., Boss E., Jumars P., et al., 1996, *Oceanography and marine biology*, 34, 71
- Kharcha P., Kasting J., Siefert J., 2005, *Geobiology*, 3, 53
- Kiang N. Y., Domagal-Goldman S., Parenteau M. N., Catling D. C., Fujii Y., Meadows V. S., Schwieterman E. W., Walker S. I., 2018, *Astrobiology*, 18, 619
- Kral T. A., Brink K. M., Miller S. L., McKay C. P., 1998, *Origins of Life and Evolution of the Biosphere*, 28, 311
- Krissansen-Totton J., Thompson M., Galloway M. L., Fortney J. J., 2022, *Nature Astronomy*, 6(2), 189
- Leung P. M., Bay S. K., Meier D. V., Chiri E., Cowan D. A., Gillor O., Woebken D., Greening C., 2020, *Msystems*, 5, 10
- Liss P. S., Slater P., 1974, *Nature*, 247, 181
- Livingston J. H., et al., 2026, *Nature*, 649, 310
- Lovelock J. E., 1965, *Nature*, 207, 568
- Lovelock J. E., Margulis L., 1974, *Tellus*, 26, 2
- Lunine J. I., Bahcall N., 2025, Characterization of exoplanets in the James Webb Space Telescope era
- Lynch T., Wanga Y., van Brunta B., Pachecob D., Janssen P., 2019, *Journal of Theoretical Biology*, 477, 14
- Madhusudhan N., Nixon M. C., Welbanks L., Piette A. A., Booth R. A., 2020, *The Astrophysical Journal*, 891, L7
- Madhusudhan N., Piette A. A., Constantinou S., 2021, *The Astrophysical Journal*, 918, 1
- Madhusudhan N., Moses J. I., Rigby F., Barrier E., 2023a, *Faraday Discussions*, 245, 80
- Madhusudhan N., Sarkar S., Constantinou S., Holmberg M., Piette A. A., Moses J. I., 2023b, *The Astrophysical Journal Letters*, 956, L13
- Mason-Jones K., Robinson S. L., Veen G., Manzoni S., van der Putten W. H., 2022, *The ISME Journal*, 16, 617
- Meadows V. S., et al., 2018, *Astrobiology*, 18
- Michał B., Gagat P., Jabłoński S., Chilimoniuk J., Gaworski M., Mackiewicz P., Marcin Ł., 2018, *Environmental microbiology reports*, 10, 378
- Miller-Ricci E., Seager S., Sasselov D., 2009, *The Astrophysical Journal*, 690, 1056
- Moger-Reischer R. Z., et al., 2023, *Nature*, 620, 122
- Montet B. T., et al., 2015, *The Astrophysical Journal*, 809, 25
- Nicholson A. E., Daines S. J., Mayne N. J., Eager-Nash J. K., Lenton T. M., Kohary K., 2022, *Monthly Notices of the Royal Astronomical Society*, 517, 222
- Ortega-Arzola E., Higgins P. M., Cockell C. S., 2024, *Scientific Reports*, 14, 5267
- Pahlow M., Riebesell U., Wolf-Gladrow D. A., 1997, *Limnology and Oceanography*, 42, 1660
- Pasciak W. J., Gavis J., 1974, *Limnology and Oceanography*, 19, 881
- Pasciak W. J., Gavis J., 1975, *Limnology and Oceanography*, 20, 604
- Pavlova M., Asaturova A., Kozitsyn A., 2022, *Biology Bulletin Reviews*, 12, 254
- Quanz S. P., et al., 2022, *Astronomy and Astrophysics*, 664, A21
- Rowe A. R., Xu S., Gardel E., Bose A., Girguis P., Amend J. P., El-Naggar M. Y., 2019, *MBio*, 10, 10
- Roy P.-A., Benneke B., Piaulet C., Coulombe L.-P., Fournier-Tondreau M., Lafreniere D., 2024, *AAS/Division for Extreme Solar Systems Abstracts*, 56, 502
- Savanov I., Shematovich V., 2021, *Astrophysical Bulletin*, 76, 450
- Seager S., Bains W., Hu R., 2013, *The Astrophysical Journal*, 775, 104
- Seager S., Welbanks L., Ellerbroek L., Bains W., Petkowski J. J., 2025, *Proceedings of the National Academy of Sciences*, 122, e2416188122
- Segura A., Kasting J. F., Meadows V., Cohen M., Scalo J., Crisp D., Butler R. A., Tinetti G., 2005, *Astrobiology*, 5, 706
- Servais P., Billen G., Vives Rego J., 1985, *American Society for Microbiology*, 49, 1448
- Shorttle O., Jordan S., Nicholls H., Lichtenberg T., Bower D. J., 2024, *The Astrophysical Journal Letters*, 962, L8
- Snellen I. A. G., et al., 2021, *Experimental Astronomy*
- Sterzik M. F., Bagnulo S., Palle E., 2012, *Nature*, 483, 64
- TRAPPIST-1 JWST Community Initiative 2024, *Nature Astronomy*, 8, 810
- Thompson M. A., Krissansen-Totton J., Wogan N., Telus M., Fortney J. J., 2022, *Proceedings of the National Academy of Sciences*, 119, e2117933119
- Tsiaras A., Waldmann I. P., Tinetti G., Tennyson J., Yurchenko S. N., 2019, *Nature Astronomy*, 3, 1086
- Vitas M., Dobovišek A., 2019, *Origins of Life and Evolution of Biospheres*, 49, 77
- Walker J., 1977, *Evolution of the Atmosphere Macmillan*. New York
- Wang S., Zhou T., Pan Z., Trusler J. M., 2023, *Journal of Chemical & Engineering Data*, 68, 1313
- Weissman J. L., Hou S., Fuhrman J. A., 2021, *Proceedings of the National Academy of Sciences*, 118, e2016810118
- West A. J., Galy A., Bickle M., 2005, *Earth and Planetary Science Letters*, 235, 211
- Wogan N., Krissansen-Totton J., Catling D. C., 2020, *The Planetary Science Journal*, 1, 58
- Wogan N. F., Batalha N. E., Zahnle K. J., Krissansen-Totton J., Tsai S.-M., Hu R., 2024, *ApJ*, 963, L7
- Wu R., et al., 2024, *npj Biofilms Microbiomes*, 10, 87
- Zhang Y., Chen Y., Zhan T., Zheng Y., Zheng X., He M., 2018, *Fluid Phase Equilibria*, 474, 126
- Zhu W., Petrovich C., Wu Y., Dong S., Xie J., 2018, *The Astrophysical Journal*, 860, 101

Chemical	Piston velocity ( $m s^{-1}$ )	Diffusivity ( $m^2 s^{-1}$ )	Solubility ( $mol L^{-1} bar^{-1}$ )
$CO_2$	$6.7 \times 10^{-4}$	$2.67 \times 10^{-8} \alpha$	$0.035 \beta$
$H_2$	$1.3 \times 10^{-4} *$	$5.0 \times 10^{-9} *$	$7.8 \times 10^{-4} *$
$CH_4$	$4.5 \times 10^{-5} *$	$1.8 \times 10^{-9} *$	$1.4 \times 10^{-3} *$

**Table A1.** Parameter values for air-ocean exchange of  $CO_2$ ,  $H_2$ , and  $CH_4$ . Values marked with a \* are taken from [Kharecha et al. \(2005\)](#),  $\alpha$  from [Zhang et al. \(2018\)](#), and  $\beta$  from <https://webbook.nist.gov/chemistry/>. Piston velocities are calculated assuming a stagnant boundary layer thickness of  $z_{film} = 40 \mu m$ . We assume a fixed temperature of  $25^\circ C$  when calculating the gas exchange between the atmosphere and ocean.

## APPENDIX A: ADDITIONAL MATERIAL

In this Appendix we include further details of the model, including results justifying the model assumptions made and including additional data to support our conclusions. The section order follows the order in which they are referenced in the main article.

### A1 Ocean-atmosphere gas exchange

Section 2.1.2 briefly explains the exchange of gas between the atmosphere and ocean in our model. The rate of exchange of gases between the ocean and the atmosphere is calculated following the stagnant layer boundary model ([Liss & Slater 1974](#)). For any chemical the rate of exchange of molecules between the ocean and atmosphere is calculated from the relative concentration of the gas in the ocean and in the atmosphere, given by

$$\Phi_X = v_p \cdot (\alpha(X) \cdot pX - [X]_{aq}), \quad (A1)$$

where  $\Phi_x$  is the flux of chemical  $X$  from the atmosphere into the ocean (here, given in terms of moles),  $v_p$  is the piston velocity of the chemical  $X$ ,  $\alpha(X)$  is the solubility of chemical  $X$  (the Henry's law coefficient),  $pX$  is the partial pressure of  $X$  (in bars) and  $[X]_{aq}$  is the dissolved concentration of  $X$  in  $mol/m^3$ .  $v_p$  is calculated by dividing the diffusivity of  $X$  by the thickness of the stagnant layer film which we assume to be  $z_{film} = 40 \mu m$  following [Kharecha et al. \(2005\)](#). Table A1 shows the values used when calculating the ocean-atmosphere exchange of gases in the model. The value of  $z_{film}$  used here is standard in models of atmosphere-ocean gas exchange on Earth, and is derived from experimental data ([Broecker et al. 1982](#); [Kharecha et al. 2005](#)). Investigating how this parameter would differ under different planetary contexts (e.g. larger planets) we leave for future work.

### A2 Removing the ATP maintenance cost of a cell

As discussed in Section 2.2 we remove the ATP cell maintenance cost and, instead of varying this parameter as was done in [Nicholson et al. \(2022\)](#), we vary the energetic cost of biosynthesis. Here we show that a changing ATP maintenance cost, or a changing biosynthesis cost affect the biosignature in the same way and thus are equivalent ways of representing the biosphere for our purposes. Using a model based on [Nicholson et al. \(2022\)](#) (see paper for full model details) and a default ATP maintenance cost value of  $c_0 = 1.75 \times 10^{-3} mol_{ATP} g^{-1} h^{-1}$  ([Lynch et al. 2019](#)) we vary the ATP cost using the values  $0.0$ ,  $0.1c_0$ ,  $0.5c_0$ ,  $c_0$ ,  $1.5c_0$  and  $2.0c_0$ . We repeat these experiments for energetic costs of generating 1 mole of ATP of  $32.5 kJ mol_{ATP}$  (the result under standard conditions) and  $75 kJ mol_{ATP}$  (the average cost for *Methanosarcina barkeri* [Lynch et al. 2019](#)). We then compare to the model outlined in the main body of this paper where there is no ATP cost but instead the energy cost of synthesising biomass is varied.

Figure A1 shows a comparison of  $atmoCH_4$  as a function of  $oceanH_2$  for the maintenance cost experiments using the original model for both  $\Delta G_{ATP} = 32.5 kJ$  and  $\Delta G_{ATP} = 75 kJ$  and for the model outlined in the main text (referred to as the 'generalised model') where the the cost of biomass synthesis  $\Delta G_{CH_2O}$  is varied instead. The data in Figure A1 follows the same curve showing that changing  $\Delta G_{ATP}$  or  $\Delta G_{CH_2O}$  have equivalent effects on the biosphere.

### A3 Calculating the default biological parameters in Section 2.2

We adopted the values for *Methanosarcina barkeri* from ([Lynch et al. 2019](#)) for use in our model. The maintenance requirement of a microbe was reported as  $2.6 \times 10^{-19} mol_{ATP} cell^{-1} s^{-1}$ . As we vary the size of our cells in this work we calculated the maintenance cost per gram of biomass. *Methanosarcina barkeri* cells have been measured as being roughly  $1 - 2 \mu m$  in length ([Rowe et al. 2019](#)) and so we use a radius of  $1 \mu m$  as our default for the cell size. An ATP maintenance cost for *Methanosarcina barkeri* cells has been measured to be  $1.75 \times 10^{-3} mol_{ATP} g_{cell}^{-1} h^{-1}$  ([Feist et al. 2006](#)) and we use this value as our default in this work. We calculate our default value for the  $CH_2O$  content of a cell per volume, by assuming a dry cell mass of  $4.44 \times 10^{-13} g$  ([Janssen et al. 1996](#)) and make the simplification that a cell consists only of  $CH_2O$ , which has a molecular mass of  $30.031 g mol^{-1}$ . We assume a perfectly spherical cell of radius  $10^{-6} m$  and this yields a  $CH_2O$  density of  $\approx 3530 mol_{CH_2O} m^{-3}$ . [Lynch et al. \(2019\)](#) use a value of  $2.36 \times 10^{13} cell mol_{ATP}^{-1}$  for the number of cells that can be made using 1 mole of ATP. Again using the assumption of a cell mass of  $4.44 \times 10^{-13} g$  ([Janssen et al. 1996](#)) and the simplification of a cell consisting entirely of  $CH_2O$  leads to a cost of building 1 mole of  $CH_2O$  being  $\approx 3 mol_{ATP}$ . In our model we assume a constant rate of removal of cells from the population due to cell death. This varies greatly between species of microbes and depends strongly on the environment. We choose to remove 2% of the population per hour as our default value and vary this significantly to capture the sensitivity of the model to this parameter.

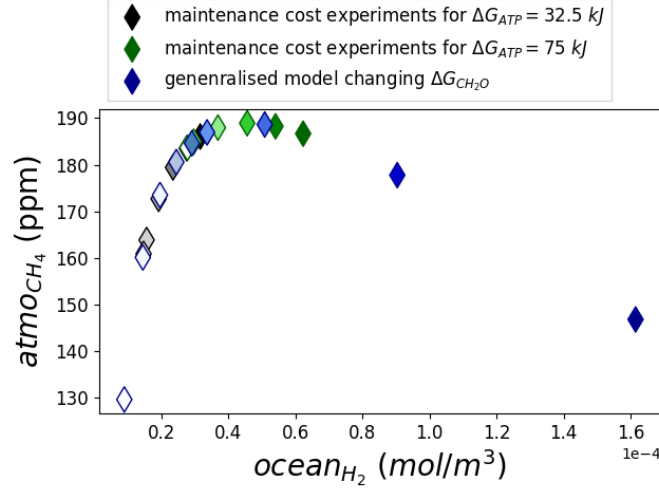


**Figure A1.** Panel b) shows a comparison between the original model  $ATP$  maintenance cost experiments for both cases where  $\Delta G_{ATP} = 32.5 \text{ kJ}$  (shown in black), and  $\Delta G_{ATP} = 75 \text{ kJ}$  (shown in green), and the generalised cell model where  $\Delta G_{CH_2O}$  is varied (data shown in blue). For all data points the default values for cell size, cell protein density and cell death rate are those listed in Table 2.

#### A4 Model time steps

As described in Section 2.3 the model is initially run abiotically for 20,000 years before seeding with life to allow the atmosphere and ocean to reach equilibrium. Life is then seeded at  $t = 20,000$  years and the model is run for a further 20,000 years.

The model iteration is described by the following sequence.

- (i) update atmospheric  $H_2$ ,  $CO_2$ , and  $CH_4$  due to inflows from abiotic sources, and outflows due to the processes outlined in Sections 2
- (ii) calculate the transfer of  $H_2$ ,  $CO_2$ , and  $CH_4$  between the atmosphere and the ocean
- (iii) for  $365 \times 60$  steps, each representing an hour:
  - (a) calculate the energy obtained from  $1 \text{ mol}$  of  $H_2$  as per Equation 2
  - (b) calculate  $H_2$  available to a cell as per Equation 5 multiplied by current population of the biosphere
  - (c) mol of  $H_2$  required for energy generation per mol of  $H_2$  converted to biomass is given by Equation 13
  - (d) assign available  $H_2$  to energy generation or biomass as per ratio
  - (e) add created biomass to the biomass of biosphere
  - (f) amount of  $CH_4$  generated by biosphere is  $4 \times H_2$  used for energy
  - (g) update the ocean concentrations of  $H_2$ ,  $CO_2$ , and  $CH_4$  due to biological activity

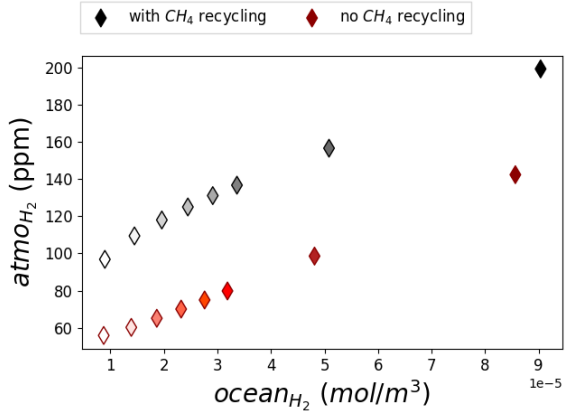
#### A5 The effect of methane recycling on the model dynamics

In Section 3.2 we showed that two different levels of atmospheric methane were possible for the same influx of  $H_2$  to the ocean. This is due to the treatment of  $CH_4$  and  $H_2$  in the atmosphere.

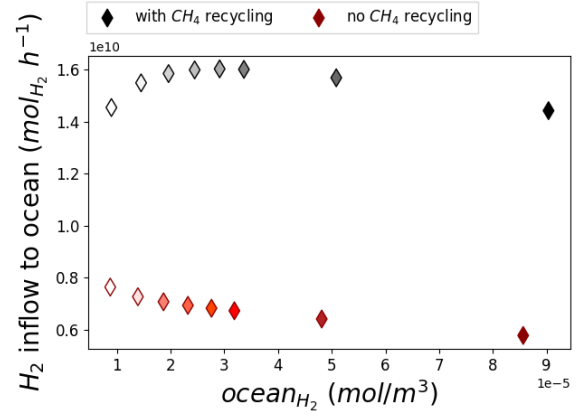
Methane recycling in the atmosphere, as described in Section 2 and the dependence of  $H_2$  loss from the top of the atmosphere on both the quantity of  $H_2$  and  $CH_4$  in the atmosphere lead to a non-linear relationship between the level of  $H_2$  in the atmosphere and the concentration of  $H_2$  in the ocean. The effect of methane recycling on the model dynamics is larger than that of  $H_2$  loss, with the recycling contributing to the peak in  $atmoCH_4$  seen in Figure 5. This is as effectively adds an additional source of  $H_2$  to the atmosphere on top of the abiotic influx.

Figure A2a shows the level of  $H_2$  in the atmosphere as a function of the concentration of  $H_2$  in the ocean for scenarios both with and without  $CH_4$  recycling. For the experiments without  $CH_4$  recycling (the red data in Figure A2) the same amount of  $CH_4$  is removed each timestep, however instead of being recycled into  $H_2$  it is simply removed from the atmosphere. Figure A2a shows that with  $CH_4$  recycling the relationship between  $atmoH_2$  and  $oceanH_2$  is non-linear. Figure A2b shows the same data but for the rate of  $H_2$  inflow to the ocean against  $oceanH_2$ . Without  $CH_4$  recycling the  $H_2$  inflow decreases as  $oceanH_2$  increases, however with  $CH_4$  recycling the flow of  $H_2$  to the ocean initially increases before decreasing after  $oceanH_2 \approx 3 \times 10^{-5} \text{ mol/m}^3$ . The peak in  $atmoCH_4$  is not solely down to this behaviour and occurs in the absence of methane recycling. Figure A2c shows  $atmoCH_4$  as a function of  $oceanH_2$  for experiments with and without methane recycling and a peak in  $atmoCH_4$  is seen in both, although  $atmoCH_4$  peaks earlier without recycling at  $oceanH_2 \approx 3 \times 10^{-5} \text{ mol/m}^3$  as a function of  $oceanH_2 \approx 5 \times 10^{-5} \text{ mol/m}^3$  with methane recycling. Figure A2d shows  $atmoCH_4$  as a function of  $H_2$  inflow to the ocean for experiments both with and without methane recycling and shows that without methane recycling only one  $atmoCH_4$  scenario is possible for each  $H_2$  inflow rate.

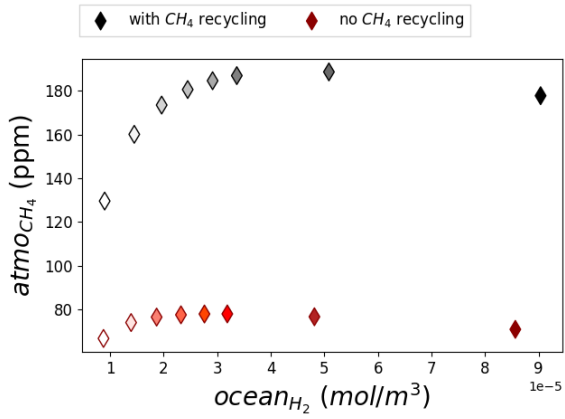
This paper has been typeset from a  $\text{\TeX}/\text{\LaTeX}$  file prepared by the author.



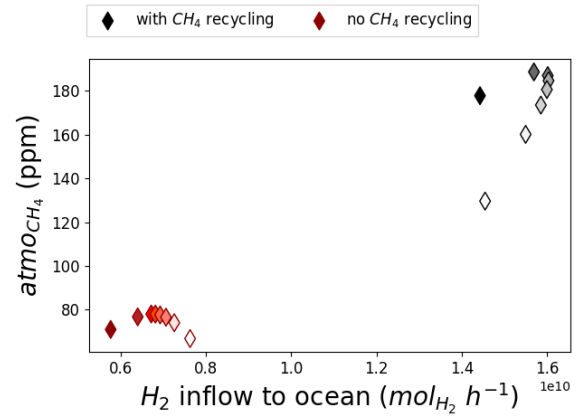
(a) Level of atmospheric  $H_2$  as a function of the concentration of  $H_2$  in the ocean.



(b) Rate of  $H_2$  inflow into the ocean as a function of the concentration of  $H_2$  in the ocean.



(c) Level of atmospheric  $CH_4$  as a function of the concentration of  $H_2$  in the ocean.



(d) Level of atmospheric  $CH_4$  as a function of the rate of  $H_2$  inflow into to the ocean.

**Figure A2.** Panels showing data from experiments with differing  $CH_2O$  synthesis costs both with methane recycling as described in Section 2, shown in black, and without methane recycling, shown in red, where instead the same quantity of methane is removed from the atmosphere each timestep. For all data  $\Delta G_{CH_4}$  is given by Equation 2. Marker colour saturation indicates the parameter value for  $CH_2O$  synthesis cost with a darker marker indicating a higher  $CH_2O$  cost.